Compton Scatter and X-ray Crosstalk and the Use of Very Thin Intercrystal Septa in High-Resolution PET Detectors

Craig S. Levin, *Member, IEEE,* Martin P. Tornai, Simon R. Cherry, *Member, IEEE,* Lawrence R. MacDonald, and Edward J. Hoffman, *Senior Member, IEEE*

***Abstract*—To improve spatial resolution, positron emission tomography (PET) systems are being developed with finer detector elements. Unfortunately, using a smaller crystal size increases intercrystal Compton scatter and X-ray escape crosstalk, causing positioning errors that can lead to degradation of image contrast. We investigated the use of extremely thin ($\leq$300 μm) lead strips for passive shielding of this intercrystal crosstalk. Using annihilation gamma rays and small (2- and 3-mm wide) Bismuth Germanate (BGO) crystal detectors in coincidence, crosstalk studies were performed with either two small adjacent crystals [(one-dimensional) (1-D)] or one crystal inside a volume of BGO [(two-dimensional) (2-D)]. The fraction of Compton scattered events from one crystal into an adjacent one was reduced, on average, by a factor of 3.2 (2.2) in the 1-D experiment and by a factor of 3.0 (2.1) in 2-D one, with a 300 (150)-μm-thick lead strip in between the crystals and a 300–700-keV energy window in both crystals. We could not measure a reduction in bismuth X-ray crosstalk with the use of lead septa due to the production of lead X-rays of similar energy. The full-width at half-maximum (FWHM) of the coincident point-spread function (CPSF) was not significantly different for the 1- and 2-D studies, with or without the different septa in place. However, the FWTM was roughly 20% smaller with the 300-μm lead shielding in place. These results indicate that intercrystal crosstalk does not affect the positioning resolution at FWHM, but does affect the tails of the CPSF. Thus, without introducing any additional dead area, an insertion of very thin lead strips can reduce the extent of positioning errors. Reducing the intercrystal crosstalk in a high-resolution PET detector array could potentially improve tomographic image contrast in situations where intercrystal crosstalk plays a significant role in event mispositioning.**

***Index Terms*—Compton scatter, detector crosstalk, intercrystal septa, PET detectors, scintillation crystals, X-ray escape.**

I. Introduction

CURRENT advances in positron emission tomography (PET) detector technology have resulted in and are moving toward the development of systems with smaller detector elements designed to further improve spatial resolution. Unfortunately, utilizing smaller crystal sizes leads to a higher fraction of intercrystal crosstalk due to Compton scattering. It has been suggested that intercrystal scattering is the primary cause of event mispositioning in high-resolution block detectors used in commercial PET systems [1]. Similar crosstalk effects occur in high-resolution discrete-crystal designs [2]–[4].

For $\leq$3-mm-wide crystals, we also have observed that bismuth K-shell X-ray and, to a lesser degree, electron escape crosstalk, also play a role. These low-energy effects result from the incomplete energy deposition of a gamma ray interaction in a crystal. The $1/e$ length of an 80-keV bismuth X-ray in BGO is approximately 0.2 mm. From UCLA Monte Carlo studies, the average range of a 511-keV photoelectron in BGO is roughly 0.1 mm. Because 511-keV gamma ray interactions result in both Compton and photo-electron production, most electrons created will have energies much less than 511 keV. In addition, because an electron deposits its energy continuously in the crystal, the remaining escape energy will be low, on average. Thus, the electron escape contribution of the low energy crosstalk will be small in comparison to that due to the 80-keV bismuth escape X-ray.

The conventional method used to reduce the effect of Compton scattering is energy thresholding on the photopeak. However, this method is somewhat limited when the energy resolution is poor, as is the case for systems using BGO, and ultimately reduces the system sensitivity. We investigated the use of extremely thin lead strips ($\leq$0.3 mm) for passive shielding of intercrystal crosstalk using measurements with a ^{22}Na source of 511-keV annihilation photons and small, 2- and 3-mm width, BGO crystal detectors in coincidence. Such fine septa can be inserted in between crystals in PET detector designs without reducing the packing fraction or introducing a dead area. These designs typically already have 250–400-μm intercrystal spaces for the reflector, and the amount of the reflector can be reduced with little loss in light output. Insertion of lead shielding is much simpler in discrete-crystal PET detector designs.

In previous work [5]–[11], intercrystal septa were, for the most part, introduced in the context of improving the spatial resolution uniformity across the imaging area (camera field of view) in conjunction with wedge-shaped or tapered crystals. In those investigations, larger crystal ($\geq$4 mm) and septa ($\geq$1 mm) widths were used. The implementation of these relatively thick septa necessarily reduced the total geometrical efficiency or ring sensitivity by reducing the crystal packing fraction. It was concluded that the benefits of improved spatial

Manuscript received December 1, 1995; revised January 5, 1997. This work was supported by the NIH under Grants T32 CA09092 and R01-CA61037 and the DOE under Grant DE-FC03-87-ER 60615.

The authors are with the Division of Nuclear Medicine and Biophysics and Imaging Sciences Division, Crump Institute for Biological Imaging, UCLA School of Medicine, Los Angeles, CA 90095–6948 USA.

Publisher Item Identifier S 0018-9499(97)02796-2.

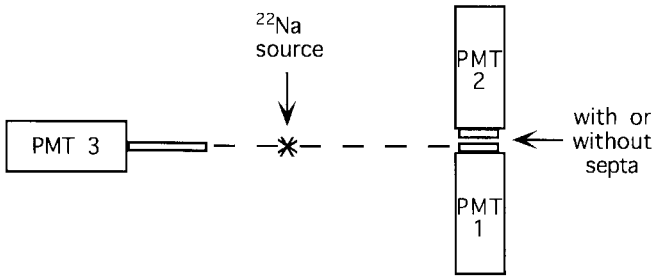

Fig. 1. Schematic of top view of setup for the 1-D experiment. PMT 1 and 3 coupled to small crystals (referred to as D1 and D3, respectively) are in coincidence.

resolution uniformity did not outweigh the disadvantages of large sensitivity loss.

The extent of mispositioning errors due to Compton scatter and X-ray crosstalk depends somewhat on the readout technique used for positioning. In a multiplexed design where the light from many crystals is read by a few channels, such as the SIEMENS EXACT HR PLUS block detector [1], the positioning is obtained by light sharing and a suitable weighted mean of four photomultiplier tube (PMT) signals. In this design, light sharing is an additional source of crosstalk due to the limited number of photons available for positioning each event [12]. Other designs [3] use resistive charge division instead of light sharing for the multiplexing of many discrete, optically isolated crystal-PMT channels and obtain positioning in an analogous manner. In these multiplexed designs, the deposition of energy in more than one crystal per event causes mispositioning of that event since all energy deposited in the array is used for the crystal position identification. The major energy threshold discrimination is performed on the sum of all the energy deposited. If this total energy is within a predefined window about the photopeak, that event is accepted.

The mispositioning error of an event due to X-ray or Compton scatter crosstalk in multiplexed systems depends on the ratio between the light signal produced in the correct crystal to that in the other crystals in the array. For example, consider an array consisting of two adjacent crystals: if 430 keV is deposited in the correct detector, and 80 keV from a bismuth escape X-ray in the adjacent one, the center of mass of the signal (relative to the midpoint) will be approximately at $0.69 \times w/2$, where w is the crystal width. For this event in the one-dimensional (1-D) array, this would translate to a $0.31 \times w/2$ mispositioning of that event from X-ray crosstalk. There will also be inherent positioning errors due to light sharing or charge division. Higher energy Compton scatter crosstalk events will produce larger positioning errors (larger shift in signal centroid). With multicrystal arrays, Compton crosstalk can occur further away from the correct crystal producing larger positioning errors.

In nonmultiplexed, single crystal-single photodetector designs the readout of each crystal is independent of the others. One may then put a given hardware energy threshold separately on each channel in the array. In that case, low energy crosstalk, such as, from bismuth X-ray escape between crystals, is not as important, and better intercrystal crosstalk rejection is possible. If desired, events in which more than two crystals are hit can be vetoed (with a large reduction in sensitivity, however). The extent of the mispositioning here depends mostly on the probability of 511-keV gamma ray Compton scatter into another crystal with energy deposition above a certain energy threshold (300 keV, for example).

We will use different energy thresholds to study the contribution of intercrystal crosstalk of different energies and see how thin lead shielding affects these measurements.

II. Materials and Methods

A. 1-D Experiment

Experiments were performed using two different thicknesses of lead intercrystal septa, 0.15 and 0.30 mm, placed in between two crystals, for both $2 \times 2 \times 10$ and $3 \times 3 \times 30$ mm^3 crystal sizes. Fig. 1 shows a top-down schematic drawing of the 1-D experimental setup. Two crystals of the same size were coupled sideways, for better light collection efficiency, with optical grease to two separate 1.5-in diameter RCA PMT's. Three layers of fine teflon tape covered the nondetecting faces of each crystal, and the unused PMT area was covered with black tape. These two PMT's with the crystals, designated D1 and D2, were then pressed together, face on, so that the side faces of the crystals were in line with each other, with or without the thin lead septa in place. There was no measurable light leak between crystals. A third BGO crystal ($2 \times 2 \times 30$ mm^3) was coupled to another PMT end on and covered with teflon and black tape (D3). This third crystal was used as the electronic back-collimating detector and was placed approximately 20 cm away from the other two detectors so that the axis of the third crystal was in line with the axis of D1. There was approximately 0.3 mm of spacing maintained between crystals D1 and D2.

The data acquisition scheme was as follows: the outputs from all three detectors were first amplified. Signals from D1 and D2 were split into two parts: the first set went into constant fraction discriminators (TENNELEC TC454, $\leq$10 ns gate for both channels) with a low threshold just above the noise, then into a coincidence unit (EG&G C315) followed by a gate and delay generator (EG&G 416A); the second set of signals were amplified and shaped (ORTEC 855, 1.5-μs shaping time) and digitized (BiRa 907). The digitizers were triggered on a coincidence between D3 and D1 (see Fig. 1). Digitized detector values of D1 and D2 were collected in list mode on a Macintosh IIfx computer through a GPIB interface to CAMAC via LabView (National Instruments).

A ^{22}Na source ($\sim$20μCi), positioned approximately 8 cm from D3, was moved perpendicular to the line between D3 and D1 in 0.5-mm steps, and the coincident point-spread function (CPSF) was measured with or without the thin lead strips in place. Source size and positron range in the plastic source holder are roughly 1 and 0.6 mm, respectively. Events observed in D2 when D1 and D3 are set in coincidence are considered to be a result of intercrystal crosstalk (Compton scatter, bismuth X-ray, or electron escape). In list mode, all energy depositions in D1 and D2 were accepted, and various upper and lower energy thresholds were applied in post-

processing. Data at various source positions were collected for the same time duration.

We define *scatter fraction* as the ratio of the number of events recorded in D2 to those in D1 for a given common energy threshold in both detectors and source position. We note that this definition of scatter fraction might be most appropriate when the electronically collimated source is directly positioned over D1, the crystal of interest. Because we are interested in the CPSF, we have loosely extended this definition of scatter fraction to include those source positions where it is more likely that the gamma ray is interacting in D2 first before scattering into D1. Remember, D1 must be hit for a trigger. The *scatter fraction reduction factor* is defined as the ratio of scatter fraction without to that with intercrystal septa in place between the two crystals. These definitions represent an average using the total number of counts in the measured energy spectrum of D1 and D2 above a given threshold. For example, if a 300-keV threshold is chosen in both detectors, then for a given event at most one detector per event can have $>$ 300 keV deposited within (511-keV maximum) and count in our definition of scatter fraction. For lower energy thresholds, such as 150 keV, both detectors can contribute to the measure of scatter fraction.

For source positions collimated directly over D1, we also calculated the ratio $R = (d1 - d2)/(d1 + d2)$ for each event, where $d1$ and $d2$ represent the pulse heights measured from the respective detectors. This ratio, R, is analogous to that used for positioning in multiplexed crystal array designs. Without scatter or X-ray crosstalk, this ratio R would always be one.

B. Two-Dimensional Experiment

Fig. 2 shows a schematic of the experimental setup used to measure the effects of completely surrounding a $2 \times 2 \times 30$ mm^3 crystal with lead septa and a volume of BGO. Only D1 and D2 are shown in Fig. 2. The general concept is the same as in the 1-D experiment except D1 now has a volume of BGO scatter media surrounding it, in an attempt to simulate a full detector array. The back-collimating detector, D3, is approximately 13 cm away from D1, and the ^{22}Na source half-way between the two. As seen in Fig. 2, the scintillation light from the two large BGO crystals that comprise D2, and which surround D1, is read from the top with a PMT. Again the source was moved perpendicular to the D1-D3 line in 0.5-mm steps, and the CPSF and scatter fraction were measured with and without lead septa surrounding D1.

Two additional effects were studied with the 2-D experiment: the contribution to the intercrystal crosstalk due to the 80-keV bismuth K-shell X-ray, and, possibly, electron escape. We note that electron escape will effect crosstalk, at best, only for interactions within a 0.1-mm perimeter of a crystal (19% of the cross-sectional area of a 2-mm-wide crystal). On average, an 80-keV bismuth X-ray will play a role within the outer 0.2 mm of the same crystal (36% of the cross-sectional area of a 2-mm-wide BGO crystal). Thus, the 80-keV bismuth X-ray escape will play a dominant role in low energy crosstalk (see Section I). With a 150-keV threshold set on D1 the total number of counts in D2 for 57–97- and 30–125-keV energy windows were measured for five collimated source positions over D1. The electron escape events deposit a continuum of energies weighted toward lower energies. The second energy window will thus encompass a larger proportion of electron escape events. We will use the crosstalk fraction measured with this latter window to roughly assess the combined contribution of escaped X-rays and electrons. For the smaller (57–97 keV) energy window, we will assume the counts are due mainly to bismuth X-ray crosstalk. The ratio of the number of events observed in D2 within these energy windows to that in D1 is the fraction of events that may be mispositioned due to low energy sources of cross talk.

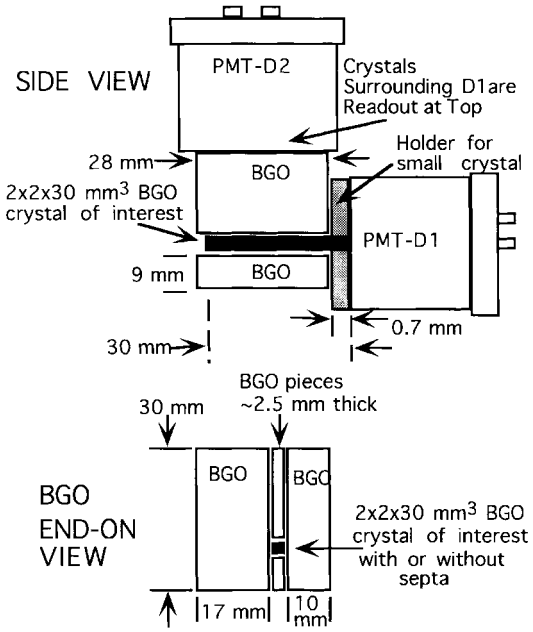

Fig. 2. D1/D2 portion of the 2-D experiment.

III. Results

A. 1-D Experiment: Point-Spread Function

Fig. 3 shows the CPSF measured in D1 and crosstalk into D2 for a 300-keV lower and 700-keV upper energy threshold in each of D1 and D2 ($2 \times 2 \times 10$ mm^3) with and without a 0.3-mm lead strip in place for the 1-D experiment. The full-width at half-maximum (FWHM) of the CPSF of D1 (1.54 mm) was measured to be only 3% narrower (only one side has the adjacent crystal) with the 0.3-mm septa in place. Note the different peak positions of the CPSF of D1 and D2. The maximum of the CPSF of D1 occurs where the source position is in line with the center of the crystal. D1 is located between positions 0.5 and 2.5 mm. Because D1 must be hit for the trigger, the maximum response of D2 is shifted to the left from its crystal center. Fig. 4 shows the corresponding full energy spectra (no threshold) measured in the crystals with and without the 0.3-mm septa with D1 and D3 in coincidence. Note the effect of the 80-keV bismuth X-ray in Fig. 4. Note also there is no 511-keV peak in the D2 spectrum because D1 must be hit for a trigger. The reduction of crosstalk into D2 with the use of septa is seen at all energies.

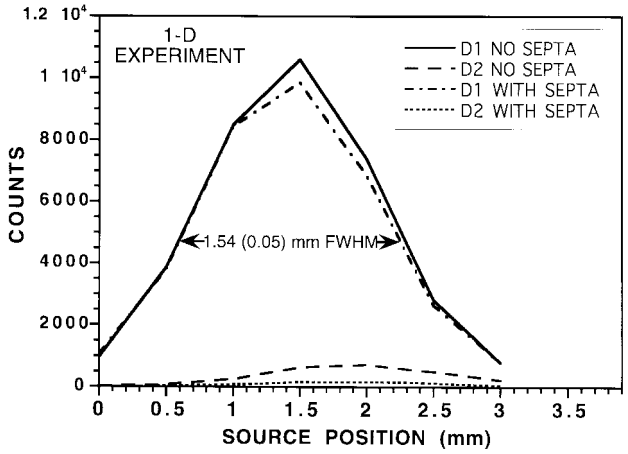

Fig. 3. Measured CPSF of D1 for a 1-mm-diameter ^{22}Na point source with and without a 0.3-mm-thick lead strip in place between D1 and D2 (see Fig. 1) for a 300-keV energy threshold. D1 must be hit to trigger the digitizers. The center of D1 is at the 1.5-mm position. D2 resides to the right of D1.

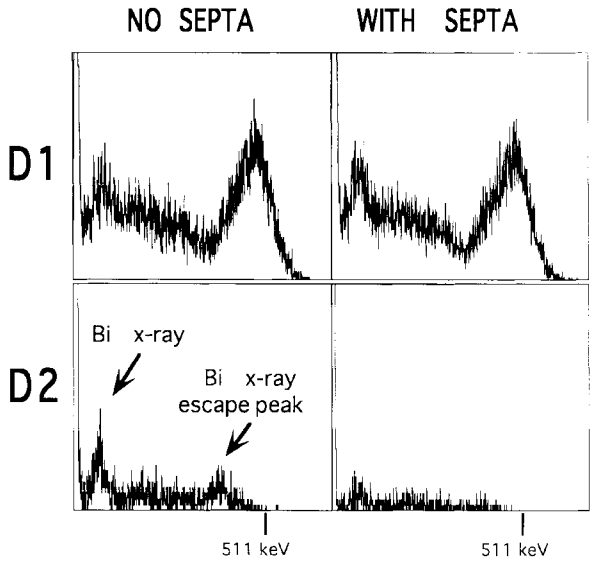

Fig. 4. Unthresholded energy spectra in both detectors when the source was electronically collimated on the center of D1 with and without the 0.3-mm lead intercrystal septa. The vertical scale of the D2 spectra shown has been enlarged by a factor of two relative to that of D1. D1 must be hit for trigger.

B. 1-D Experiment: Scatter Fraction

Fig. 5 shows the scatter fraction measured in D2 for a 300-keV lower and 700-keV upper energy threshold in each of the $2 \times 2 \times 10$ mm^3 crystals, with and without the 0.3-mm-thick septa in place as a function of source position. With this high 300-keV threshold on each detector, for a given trigger in D1, pulses from either D1 or D2, but not both, will contribute to the scatter fraction definition. We note that the definition of scatter fraction given in Section II might be most appropriate when the source position is collimated over D1, but this quantity is also shown for positions outside of D1. Position 1.5 is the center of D1. For source positions directly over D1, with a 300-keV energy threshold in each crystal, 80-keV X-ray crosstalk does not have an effect on these results.

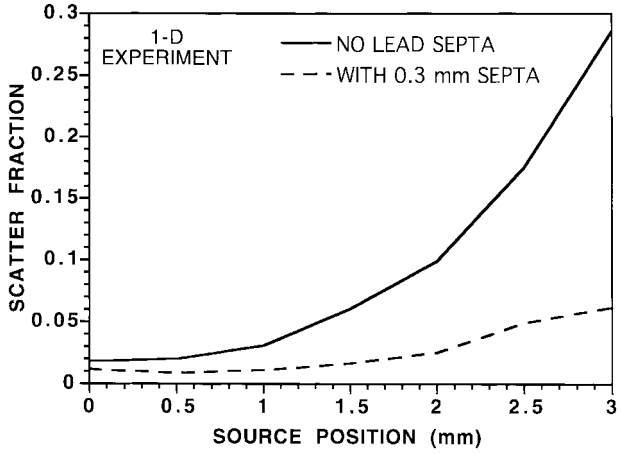

Fig. 5. Scatter fraction versus source position with and without the 0.3-mm lead septa (300-keV threshold in D1 and D2).

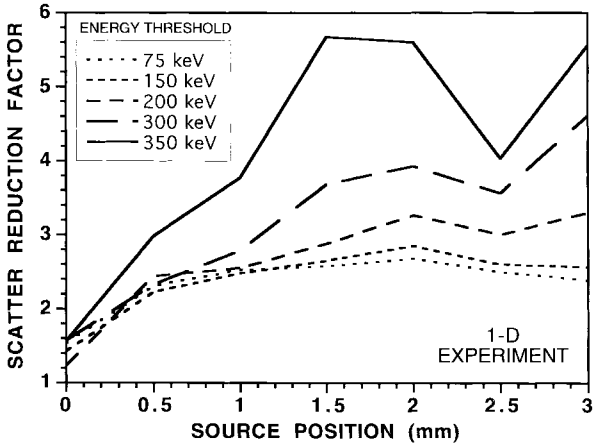

Fig. 6. Scatter fraction reduction factor measured using the 0.3-mm-thick intercrystal lead septa as a function of source position for various energy thresholds. The dip seen is approximately at the position of the septa.

Fig. 6 shows the scatter fraction reduction factor achieved with the 0.3-mm lead strip in place as a function of various source positions and energy thresholds. Results for the 0.15-mm septa are not shown here, for simplicity. For a 300-keV energy threshold, and source positions over D1, we found that the fraction of scattered events into an adjacent crystal was reduced, on average, by a factor of 3.2 (2.1) when there was a 0.30 (0.15)-mm thick lead strip in place. In general, this reduction factor depended on energy threshold (see energy spectra in Fig. 4) and source position. With the lead strips in place between larger $3 \times 3 \times 30$ mm^3 crystals, we found similar results for the scatter fraction reduction factor: the larger crystals had, within 10%, approximately the same scatter fraction above a 300-keV energy threshold for points directly over the D1 crystal as for the $2 \times 2 \times 10$ mm^3 crystals.

In Fig. 7 we show a different way of representing the scatter data. Let $d1$ and $d2$ be the digitized pulse heights from D1 and D2, respectively, for a given event. Fig. 7 shows a histogram of the ratio $(d1 - d2)/(d1 + d2)$ with and without the 0.3-mm septa present for a source position centered on D1. This ratio is a two-crystal analogy of the positioning algorithm used in multiplexed (light or charge

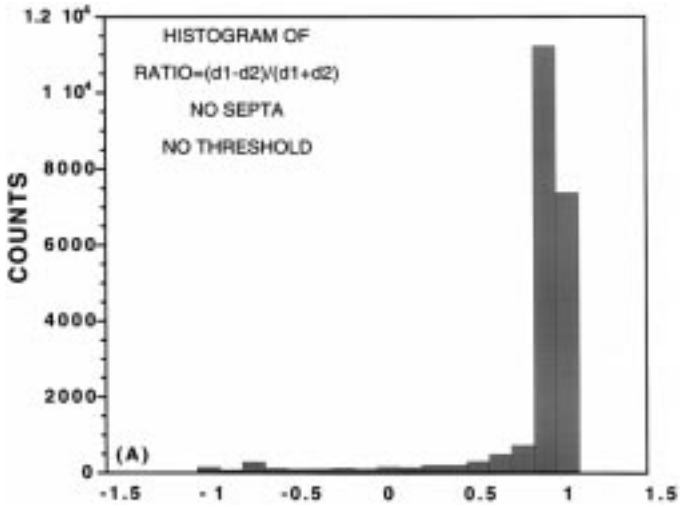

(a)

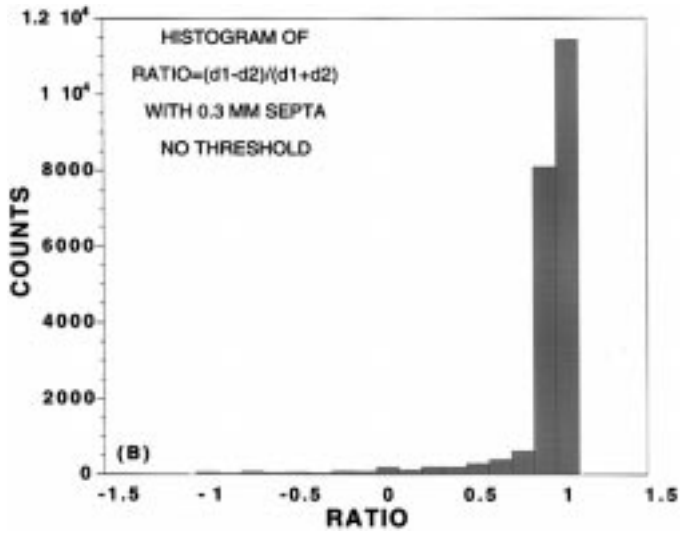

(b)

Fig. 7. Plot of the difference between the signals measured in D1 and D2 normalized by the total signal for (a) no septa and (b) with 0.3-mm septa for the 1-D experiment (Fig. 1). The presence of the septa reduces the errors in positioning. The correct position is a ratio of one. All energies were used.

sharing) PET detector array designs [1], [3], where all of the light created from all the crystals in the array is used for crystal identification/positioning and energy thresholding of an event. We see the deviation from the correct position, a ratio of one, lessens with the septa in place, including at those ratio positions near -1, where, without septa, most of the energy is deposited in the wrong crystal. From this figure one can better assess the contribution of Compton scatter and X-ray crosstalk to mispositioning errors in an array, without the presence of light sharing effects. The Compton scatter crosstalk produces larger positioning errors than do escape X-rays.

C. 2-D Experiment: Point-Spread Function

Fig. 8 shows the CPSF measured in D1 and crosstalk component seen in D2 for a 300-keV lower and 700-keV upper energy threshold in both detectors with and without the two sizes of lead septa (0.15 and 0.30 mm) in place. There is no

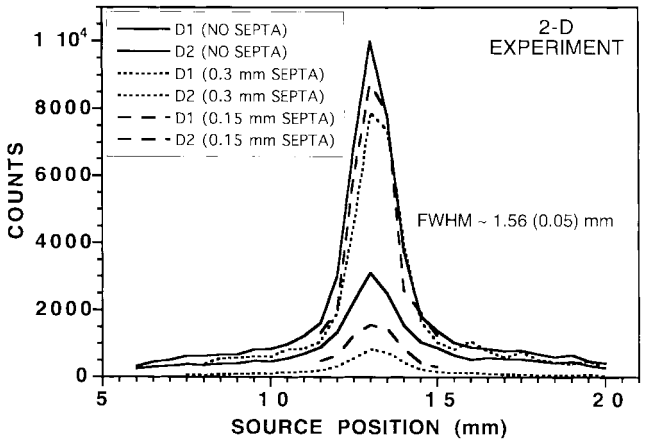

Fig. 8. CPSF measured for D1 and crosstalk measured in D2 as a function of source position without and with 0.15- and 0.3-mm-thick lead septa completely surrounding D1 (300-keV lower and 700-keV upper energy thresholds in D1 and D2). Upper three curves: response of D1; lower three curves: corresponding response of D2. D1 must be hit for trigger. D1 is centered on the 13-mm source position. D2 is a BGO volume surrounding D1 (see Fig. 2).

significant difference in the CPSF FWHM between the 1- and 2-D configurations without septa, even though there is a much greater BGO scatter volume present and nearly four times the scatter fraction. Furthermore, there is no significant change in the CPSF at FWHM with the introduction of septa. There was, however, a roughly 20% improvement in the full-width at tenth-maximum (FWTM) seen with the 0.3-mm lead present in the 2-D experiment. There is, also, a 6–8% difference in the FWHM for the profile of counts measured in D2, the "wrong" crystal. These results will be discussed in Section IV. Note that the D1 crystal is centered on the 13-mm source position. The 17-mm BGO volume (see Fig. 2) roughly begins just above the 14-mm source position in Fig. 8. The 10-mm BGO volume begins just below the 12-mm source position.

D. 2-D Experiment: Scatter Fraction

Fig. 9 displays the fractional crosstalk (a) and crosstalk reduction (b) with no septa and with 0.15- and 0.3-mm septa in place for the 2-D experiment. For source positions directly over D1 (12–14 mm), since the energy thresholds are high in this figure, the X-ray escape peak of bismuth does not contribute to this scatter fraction calculation. Remember, D1 must be hit to trigger the digitizers. The scatter fraction is improved, on average, by a factor of 3.0 (2.1) with the 0.3 (1.5)-mm septa in place. These values correspond well with those measured in the 1-D experiment. For a 300-keV energy threshold, without septa, scatter crosstalk into D2 from D1 varies from 35–47%, which agrees with results in [1] for larger, pseudo-discrete BGO crystals. The measured scatter fraction is roughly twice as large for a 150-keV threshold.

E. Crosstalk Due to X-ray and Electron Escape

Fig. 10 displays the crosstalk fraction (ratio of counts in D2 to those in D1) for a lower-energy window in D2 centered about the 77-keV bismuth X-ray with and without septa in place. Bismuth X-ray crosstalk into D2 with no septa accounts

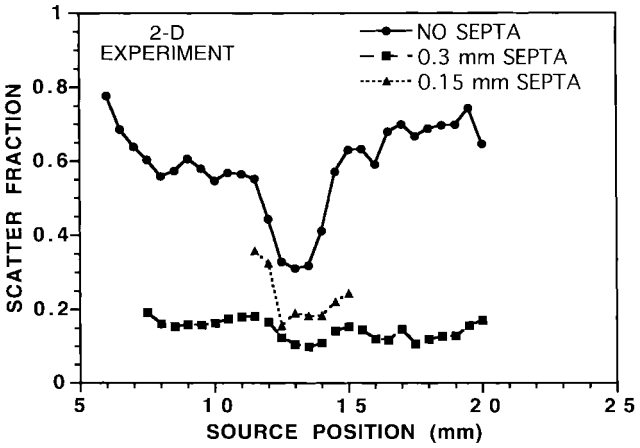

(a)

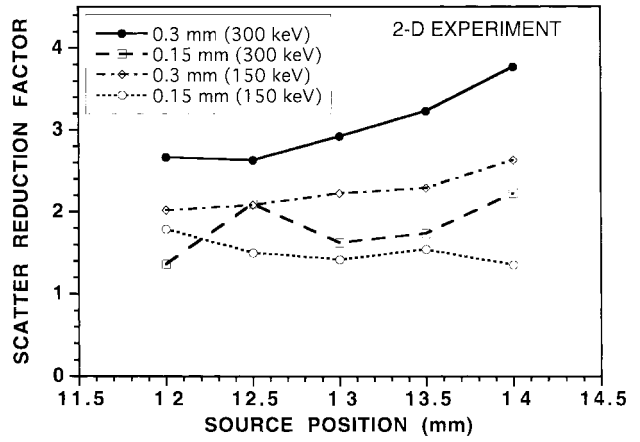

(b)

Fig. 9. (a) Scatter fraction versus source position for no septa, 0.15- and 0.3-mm lead septa (only 300-keV threshold data shown). (b) Corresponding scatter reduction factor for 150- and 300-keV thresholds. The 13-mm source position is centered on D1.

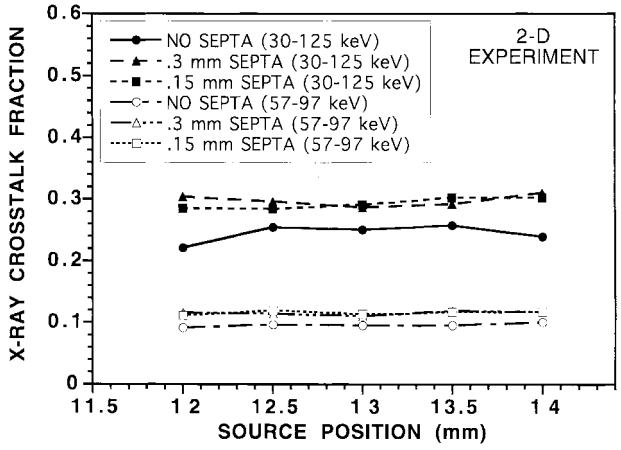

Fig. 10. X-ray and electron escape crosstalk fraction versus source position for the 2-D experiment for 57–97-keV (lower curves) and 30–125-keV (upper curves) energy windows centered on 77 keV. In both cases a lower energy threshold of 150 keV was set in D1. The presence of lead septa slightly increases crosstalk at low energies due to 80-keV lead X-rays produced.

for roughly 10% of the events registered in D1 for a 50% energy window centered about 77 keV (57–97 keV) and a lower energy threshold of 150 keV set in D1. For a 95-keV window about 77 keV the estimation of the combined X-ray and electron escape crosstalk is 20%. We note that this large window includes some low energy Compton scatter events as well so this estimation is only approximate. We observed an increase in X-ray crosstalk when 0.15- and 0.30-mm septa is used. This is due to the fact that gamma rays interacting with lead also produce 80-keV lead X-rays. Thus there will be competing effects of gamma and bismuth X-ray and electron attenuation in the lead (crosstalk reduction) and lead X-ray production. The dominant role of the lead X-ray production may explain why the X-ray crosstalk fraction does not seem to vary with source position.

IV. Discussion

We have discussed Compton scatter and X-ray and electron escape intercrystal crosstalk relevant to high resolution PET detector arrays. The latter two crosstalk sources become relevant only for $\leq$3-mm crystal widths. In fact, the probability of 77-keV X-ray absorption is higher in BGO than for lead. Detector crosstalk sources do cause positioning errors which can contribute to a reduction in tomographic image contrast. In this experiment neither crosstalk sources nor intercrystal septa appeared to affect the intrinsic resolution as measured by the FWHM of the CPSF (see Figs. 3 and 8). The FWTM, however, improved by 20% with 0.3 mm of lead shielding surrounding one crystal of interest within a 2-D array of BGO. In this experiment, the CPSF FWHM is determined by the crystal size, the size of the point source, and the positron range in the source holder. Adding a 1-mm source size, 0.6-mm ^{22}Na average positron range fluctuation, and 1-mm half-crystal width in quadrature, we arrive at an intrinsic value of 1.54-mm FWHM, which compares well with the values obtained in Sections III-A (1.54 (0.05) mm) and III-C (1.56 (0.05) mm).

Our results also indicate that with the simple insertion of very thin lead strips between $\leq$3-mm-wide crystals, the crosstalk, and, therefore, the positioning errors due to Compton scatter, can be reduced significantly. This reduction in scatter crosstalk is partially manifested by a reduction in the FWTM (the "tails" of the CPSF). The CPSF FWTM is a measure of the scatter background and affects the ability to separate individual crystals in a detector array. A tomograph ring consisting of detector arrays that measure poor individual crystal peak to valley ratios will inevitably worsen tomographic image contrast, although, perhaps not as much as from scatter within the body of the subject. This is especially true for small animal imaging, where intercrystal scatter is the dominant source of positioning errors [13]. The thin septa can be implemented in existing designs that already have gaps present [1] without reducing the crystal packing fraction. Whether a reduction in positioning errors and potential improvement in tomographic image contrast would be worth the cost increase of introducing shielding between crystals is open for debate.

There are two components of gamma "attenuation" by the intercrystal septa in our experiment: 1) energy loss in the septa and 2) energy discrimination: counts are rejected if the resulting energy is below threshold. The goal of this approach

was not to stop or attenuate 511-keV photons. The idea is that some scattered gamma rays (energy < 511 keV) will lose enough energy after traversing the lead septa, especially at small angles with respect to the crystal axis, so that the energy deposited in the secondary detector was less than a chosen energy threshold. We saw in Fig. 6 that even for low energy thresholds, the scatter crosstalk reduction factor with 0.3-mm septa is roughly 2.5 for collimated source positions over D1. We believe the effect of the thin lead here on gamma rays is somewhat analogous to that seen in the collimator of a gamma camera. For small scatter angles of entrance into the secondary crystal, the amount of lead actually traversed is greater than the actual thickness, resulting in a higher probability of gamma ray interaction within the septa. The septa will also completely absorb very low energy scattered gamma-rays and escape X-rays and electrons.

What is the relation between the scatter fraction and the FWTM of the CPSF? The CPSF FWTM measured in this experiment extends beyond the physical width of the D1 crystal by virtue of the scattering of events from D2 into D1. Remember D1 and D3 are collinear, and their coincidence defines the trigger; so for source positions electronically collimated on D2, the gamma ray is interacting in D2 before scattering into D1 (see Fig. 1, for a picture). Thus, the most appropriate definition of scatter fraction in this work, which depends on crosstalk from D1 into D2, is only weakly dependent on the CPSF FWTM. In our experiment, the average angle of entrance into a crystal and average scatter angle into the adjacent crystal may be larger when the gamma ray hits D2 first rather than D1. This larger angle scattering implies, on average, a more normal angle of incidence from D2 onto the septa, which may tend to reduce the thin septa attenuating properties. However, the larger scattering angle gamma rays have lower energy, and the BGO and lead may then possibly play a bigger role in their attenuation. Such effects might play a role in the observation of a 20% CPSF FWTM reduction using the 0.3-mm septa (300 keV threshold) and a factor of three reduction in scatter fraction and thus positioning error (see Figs. 8 and 9).

Our study focused on electronically collimated gamma rays that enter D1 parallel to the crystal axis. Will the intercrystal septa have the same effect on gamma rays that enter the crystal at more oblique angles? Will the benefits of reduced crosstalk and CPSF tails still hold? We have no answer yet to these questions. However, in brain or small children studies, normal incidence gamma rays may be a good approximation. This question of oblique incidence also has relevance to the radial elongation problem in PET. With very oblique gamma ray incidence, where multiple crystals and intercrystal septa planes are traversed, we expect that this parallax effect might be reduced. However, this improvement may also be accompanied by a reduction in sensitivity for the outer part of the field of view (FOV).

There may be an additional benefit of using intercrystal septa in situations where intercrystal detector scatter effects are significant compared to those due to scatter within the body of the subject to be imaged (as is the case for small animals). Since part of the scatter/crosstalk is passively rejected, the septa effectively reduces the need for active energy thresholding used for scatter rejection, thereby possibly increasing overall PET scanner efficiency.

The scatter crosstalk reduction results should improve with the use of tungsten as the septa material since it has a much higher gamma ray stopping power (higher Z and density, at a higher cost, however). For systems composed of lower stopping power crystals, such as Lutetium Oxyorthosilicate (LSO), the intercrystal crosstalk fraction will most likely increase. In this case, intercrystal septa may be even more useful.

REFERENCES

[1] S. R. Cherry, M. P. Tornai, C. S. Levin, S. Siegel, and E. J. Hoffman, "A comparison of PET detector modules employing rectangular and round photomultiplier tubes," *IEEE Trans. Nucl. Sci.*, vol. 42, pp. 1064–1068, Aug. 1995.

[2] W. W. Moses and S. E. Derenzo, "Design studies for a PET detector module using a PIN photodiode to measure depth of interaction," *IEEE Trans. Nucl. Sci.*, vol. 41, pp. 1441–1445, 1994.

[3] S. R. Cherry *et al*., "Optical fiber readout of scintillator arrays using a multi-channel PMT: A high resolution PET detector for animal imaging," *IEEE Trans. Nucl. Sci.*, vol. 43, pp. 1932–1937, June 1996.

[4] C. J. Marriot *et al*., "High resolution PET imaging and quantitation of pharmaceutical biodistributions in a small animal using avalanche photodiode detectors," *J. Nucl. Med.*, vol. 35, pp. 1390–1397, 1994.

[5] N. A. Keller and L. R. Lupton, "PET detector ring aperture function calculations using Monte Carlo techniques," *IEEE Trans. Nucl. Sci.*, vol. 30, pp. 676–680, Feb. 1983.

[6] J. M. Roney and C. J. Thompson, "Detector identification with four BGO crystals on a dual PMT," *IEEE Trans. Nucl. Sci.*, vol. NS-31, pp. 1022–1027, 1984.

[7] R. Lecomte, D. Schmitt, and G. Lamoureux, "Geometry study of a high resolution PET detection system using small detectors," *IEEE Trans. Nucl. Sci.*, vol. 31, pp. 556–561, Feb. 1984.

[8] T. J. Holmes and D. C. Ficke, "Analysis of positron-emission tomography scintillation-detectors with wedge faces and inter-crystal septa," *IEEE Trans. Nucl. Sci.*, vol. 32, pp. 826–830, Feb. 1985.

[9] M. Kesselberg, C. Bohm, J. E. Litton, and L. Eriksson, "Design considerations of small crystal positron camera systems," *IEEE Trans. Nucl. Sci.*, vol. 32, pp. 907–911, Feb. 1985.

[10] I. N. Weinberg, M. Dahlbom, A. Ricci, and E. J. Hoffman, "Crystal identification in modular array detectors for high spatial resolution PET," vol. SPIE 671, pp. 261–268, 1986.

[11] D. Schmitt, R. Lecomte, and E. LeBel, "Wedge-shaped scintillation crystals for positron emission tomography," *J. Nucl. Med.*, vol. 27, pp. 99–104, 1986.

[12] W. W. Moses and S. E. Derenzo, "Empirical observation of resolution degradation in positron emission tomographs utilizing block detectors," *J. Nucl. Med.*, vol. 34, p. 101, 1993.

[13] M. Bentourkia, P. Msaki, J. Cadorette, and R. Lecomte, "Object and detector scatter-function dependence on energy and position in high resolution PET," *IEEE Trans. Nucl. Sci.*, vol. 42, pp. 1162–1167, 1995.